Backbone Dynamics of a Module Pair from the Ligand-Binding Domain of the LDL Receptor†

Natalia Beglova, Christopher L. North, and Stephen C. Blacklow*

Department of Pathology, Brigham and Women's Hospital and Harvard Medical School, 75 Francis Street, Boston, Massachusetts 02115

Received November 29, 2000; Revised Manuscript Received January 11, 2001

ABSTRACT: The ligand-binding domain of the LDL receptor consists of seven contiguous LDL-A modules. The fifth of these ligand-binding modules is absolutely required for recognition of both LDL and β-VLDL particles. A four-residue linker of variable sequence connects each pair of modules, except for modules four and five, which are connected by a 12-residue linker. To provide a more detailed understanding of the structural relationship in a typical pair of functionally important LDL-A repeats of the LDLR, we investigated the backbone dynamics of repeats five (LR5) and six (LR6) alone and in the context of the covalently connected LR5-6 pair. Our results reveal substantial flexibility in the four-residue linker connecting the two repeats in the LR5-6 pair. The intrinsic dynamic behavior of each repeat is essentially unchanged when the repeats are covalently connected. These observations indicate that the relative orientation of repeats in LR5-6 is not fixed. Modeled in an extended conformation, the linker can separate LR5 and LR6 by up to 15 Å, a distance that would allow substantial freedom of motion of each repeat with respect to the other in the pair.

The low-density lipoprotein receptor (LDLR; *1*−*3*)[1] is a prototype for an entire class of transmembrane receptors (*4*, *5*). Other members of this receptor family in humans include the very low-density lipoprotein receptor (*6*), apolipoprotein E receptor 2 (*7*), LDLR-related protein (*8*), and megalin (*9*). These proteins combine several types of structural units in similar arrangements, such that groups of LDL-A modules precede regions with clusters of EGF-modules and YWTD domains (*10*). Each receptor then terminates with a transmembrane segment and a cytoplasmic tail of variable length.

Despite their similar structural organization, these receptors carry out a diverse array of biological functions, including lipoprotein transport into cells (*11*, *12*), clearance of protein complexes from plasma (*13*), and transmission of extracellular signals in nervous system development (*14*, *15*). Specific ligands have been identified for each of these receptors, yet all members of the LDLR family also bind receptor-associated protein (RAP) and lipoprotein particles containing apolipoprotein E (*4*).

† Supported by NIH Grant HL61001 (to S.C.B.) and by the Armenise Center for Structural Biology at Harvard Medical School. S.C.B. is a Pew Scholar in the Biomedical Sciences.

* To whom correspondence should be addressed: Tel: (617) 732-5799. Fax: (617) 264-5296. E-mail: sblacklow@rics.bwh.harvard.edu.

[1] Abbreviations: apo, apolipoprotein; apoE-R2, apolipoprotein E receptor 2; CPMG, Carr−Purcell−Meiboom−Gill; EGF, epidermal growth factor; FH, familial hypercholesterolemia; HPLC, high-performance liquid chromatography; HSQC, heteronuclear single quantum coherence; LDL, low-density lipoprotein; LDLR, low-density lipoprotein receptor; LR, LDL-A module; LR5, LDL-A module five of the low-density lipoprotein receptor; LR6, LDL-A module six of the LDL receptor with the M243L substitution; LR5-6, the LR5-LR6 module pair; LRP, low-density lipoprotein related protein; NMR, nuclear magenetic resonance; RAP, receptor-associated protein; VLDL, very low-density lipoprotein; VLDLR, very low-density lipoprotein receptor.

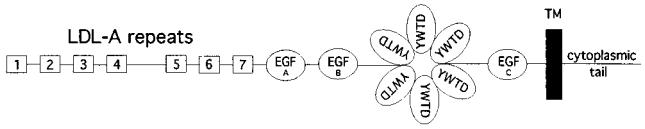

FIGURE 1: Schematic of the modular organization of the LDL receptor, illustrating the positions of LDL-A modules, EGF-like modules, and repeats containing the YWTD motif.

Ligand binding by LDLR family members requires participation of the cysteine-rich LDL-A repeats (*16*, *17*). Each LDL-A repeat is about 40 residues long and contains six cysteines that form three disulfide bonds. Ca^{2+} is required for ligand binding (*18*, *19*), and the Ca^{2+} coordinating residues, along with the six cysteines, constitute the major conserved sequence features of LDL-A repeats.

The main function of the LDLR is to transport plasma cholesterol into cells (*11*, *20*). Mutations of the gene encoding the LDLR cause familial hypercholesterolemia (FH), a common metabolic disorder inherited in an autosomal dominant pattern (see ref *21* for a review). Elevated levels of plasma cholesterol in patients with heterozygous FH result in an increased risk for cardiovascular disease, and patients with homozygous FH, if untreated, die of coronary heart disease at an early age.

The ligand-binding domain of the LDLR consists of seven adjacent LDL-A repeats (Figure 1). The main ligands for the LDLR are lipoprotein particles containing apolipoprotein B (LDL) and apolipoprotein E (β-VLDL). Deletion of individual repeats and systematic mutation of conserved residues within each repeat demonstrated that the fifth LDL-A module of the LDLR makes critical contributions to the binding of both LDL and β-VLDL particles (*17*). Modules three through seven are essential for binding of

10.1021/bi0027276 CCC: $20.00
Published on Web 02/10/2001

LDL; in contrast, only deletion of module five prevents high-affinity binding of β-VLDL (*17*).

The structure of the fifth LDL-A module has been solved to 1.7 Å by X-ray crystallography (*22*), and solution structures have been determined for LDL-A modules 1 (*23*), 2 (*24*), and 6 (*25*) of the LDLR and for two of the LDL-A modules of the LRP (*26*, *27*). Each of these modules exhibits a similar tertiary fold organized around one bound calcium ion, which stabilizes the structure in conjunction with the three disulfide bonds. In the absence of Ca^{2+}, the LDL-A modules appear to be unstructured (*28*, *29*).

Relatively little is known regarding the orientation of LDL-A repeats within the ligand-binding domain of the LDLR and how these repeats are organized for interaction with ligands. Linkers connecting LDL-A modules comprise four residues (except for the linker between modules four and five). Short linkers are found both in proteins with a fixed orientation between adjacent domains (*30*−*32*) and in proteins with substantial interdomain mobility (*33*, *34*). Chemical shift perturbation studies of the five−six (*35*) and one−two (*36*) module pairs from the LDLR reveal that the strongest perturbations occur in the linkers connecting repeats, indicating that the backbone folds of individual modules remain unchanged in each module pair. Further characterization of the LR1-2 module pair failed to detect side chain−side chain intermodule NOE cross-peaks (*37*).

We used NMR relaxation data to evaluate the degree of flexibility in the linker between LDLR modules five and six and to compare the internal and overall dynamics of each individual module with the dynamics of the module pair. These studies are focused upon the LR5-6 module pair because deletion of either module prevents high affinity binding of LDL particles, and the presence of LR5 is crucial for high affinity binding of β-VLDL (*17*). Our results reveal substantial flexibility in the four-residue linker connecting the two repeats in the LR5-6 pair. Furthermore, the intrinsic dynamic behavior of each repeat is essentially unaltered when the repeats are connected in the LR5-6 pair. Taken together, these observations suggest that the presence of one module of the LR5-6 pair imposes little restriction on the dynamics of its neighbor in solution.

EXPERIMENTAL PROCEDURES

Sample Preparation and NMR Spectroscopy. LR5, LR6, and the LR5-6 module pair were expressed and purified in ^{15}N-labeled form as described previously (*35*). In LR6 and LR5-6, the M243L substitution was incorporated to permit cleavage of the expressed fusion protein with cyanogen bromide prior to refolding and HPLC purification (*35*). Each NMR sample contained 1 mM protein in 90% H_2O/10% D_2O, pH 5.6, and 10 mM $CaCl_2$. This calcium ion concentration, which exceeds the calcium dissociation constant by several orders of magnitude, is sufficient to ensure saturation of all Ca^{2+} binding sites (*35*).

All NMR relaxation experiments were performed at 298 K on a Bruker-600 spectrometer equipped with a triple-resonance, pulsed-field z-gradient probe. NMR data were processed using GIFA version 4.2 (*38*). Data were linear predicted in the indirect dimension and zero-filled before Fourier transformation. A suitable apodization function was applied in both dimensions. The backbone ^{1}H and ^{15}N resonance assignments of LR5, LR6, and the LR5-6 module pair were obtained previously using 3-dimensional ^{15}N edited spectra (*35*).

^{15}N-R1, ^{15}N-R2, and $\{^1H\}$-^{15}N heteronuclear NOE data were acquired using published pulse sequences (*39*). For measurements of R2, the delay between 180 degree CPMG pulses was set to 900 μs. To ensure that all R2 experiments were conducted at the same temperature, a series of 180 degree CPMG pulses and delays were included before the recycling delay such that the total number of ^{15}N refocusing pulses was the same in each R2 experiment. The strength of the 180 degree CPMG pulses was adjusted to minimize sample heating, with possible effects due to sample heating assessed by comparison of amide-proton chemical shifts in experiments with minimal and maximal relaxation delays. To confirm that the R1 and R2 experiments were conducted at the same effective temperature, amide-proton chemical shifts were compared between R1 and R2 experiments. Each series of R1 and R2 measurements consisted of 6−9 spectra with increasing ^{15}N relaxation time delays. To sample the whole range of intensity decays, the largest relaxation delay exceeded the average relaxation time by at least 3-fold. Longitudinal and transverse relaxation rates and their uncertainties were determined by nonlinear least-squares fitting of the experimentally measured resonance intensities to monoexponential decay. The public domain program GNUPLOT was used to fit the relaxation rates to the experimental data. Uncertainties in the exponential fits were estimated from the covariance matrix.

Heteronuclear NOE values were determined from spectra with and without proton saturation recorded in an interleaved manner. A repetition delay of 5 s was used for hNOE measurements; proton saturation was achieved after an initial delay of 1 s by means of a subsequent 4 s train of 120° flip-angle pulses applied at 5 ms intervals. The magnitude of the $\{^1H\}$-^{15}N heteronuclear NOE effect was calculated from the equation $\text{hNOE} = (I_s - I_u)/I_u$, where I_s and I_u are the intensities of peaks in spectra acquired with and without proton saturation, respectively. Uncertainties in the heteronuclear NOE data were estimated from the signal-to-noise values in the recorded spectra. The values of τ_m were calculated from $R2/R1$ ratios according to Kay et al. (*40*), and errors were estimated from the simulated data.

For spectral density mapping, the rate constant for heteronuclear cross-relaxation (R_{H-N}) was calculated using the expression $R_{H-N} = (\gamma N/\gamma H)*\text{hNOE}*R1$. Values of the spectral density function $J_{avg}(w_H)$ were calculated from the relaxation data using the approximation $J(w_H + w_N) = J(w_H) = J(w_H - w_N)$ (ref *41*); spectral density functions were calculated according to Peng et al. and Dayie et al. (*41*, *42*).

RESULTS

^{15}N Relaxation Data Analysis. Longitudinal (^{15}N-R1) and transverse (^{15}N-R2) relaxation rates and ^{1}H-^{15}N heteronuclear NOEs (hNOEs) were measured for 34 residues of LR5, for 38 residues of LR6 and for 70 residues of the LR5-6 pair. Spectral overlap and/or absence of cross-peaks precluded acquisition of relaxation data for D172, S173, S174, P175, S192, and P199 of LR5, for V212 and P217 of LR6, and

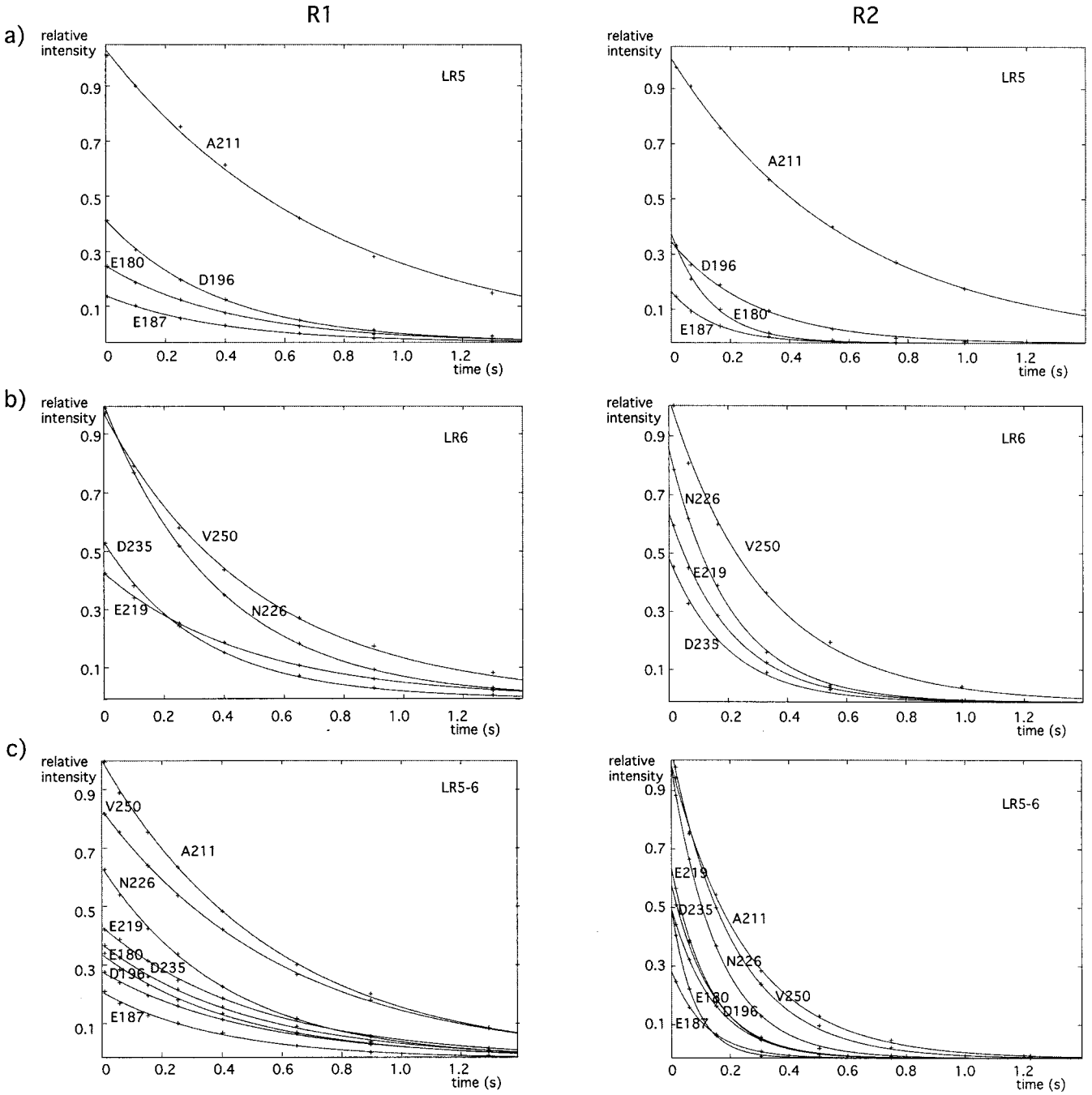

FIGURE 2: Representative plots of intensity decays used to derive the relaxation parameters *R*1 (left panels) and *R*2 (right panels) for residues in LR5 (a), LR6 (b), and LR5-6 (c). Curves represent the best fit to the data using a monoexponential decay model. Residues E180, E187, D196, and A211 from LR5 (panels a and c), and residues E219, N226, D235, and V250 from LR6 (panels b and c) are shown.

for D172, S173, P175, P199, K201, R216, P217, F220, H229, and C240 of LR5-6. Uncertainties in the exponential fits were about 2 ± 1% (average ± SD) for R1 and 3 ± 2% for R2; based on observed signal-to-noise ratios, the error in the measured hNOEs were 6 ± 4%. Representative plots illustrating monoexponential fits used to determine *R*1 and *R*2 for each molecule are illustrated in Figure 2.

We compared relaxation data measured for the backbone amides of the individual repeats with the relaxation data for the corresponding residues of the pair (Figure 3). The hNOE values are roughly uniform in the core regions, defined as the residues bounded by the first and the last cysteine of each module (Figure 3, panel a). The average hNOE values of the core residues of LR5, LR6, and the LR5-6 pair (−0.39 ± 0.13, −0.37 ± 0.10, and −0.33 ± 0.07, respectively) indicate that modules are well ordered.

^{1}H-^{15}N hNOEs are sensitive to fast pico- to nanosecond time-scale internal motions. The large negative hNOEs at the termini of LR5 and LR6 indicate that the termini in the individual repeats undergo fast internal motion. In the LR5-6 pair, a four-residue linker connects the last cysteine in LR5 to the first cysteine of LR6. The observed decrease in the hNOEs in the linker relative to the core residues of both repeats indicates that the linker residues retain substantial flexibility in the covalently connected LR5-6 pair. The values of the hNOEs are consistent with published hNOEs values for other flexible linkers (*33*, *34*). The *R*1 relaxation rates, which decrease in the linker region, correlate well with the

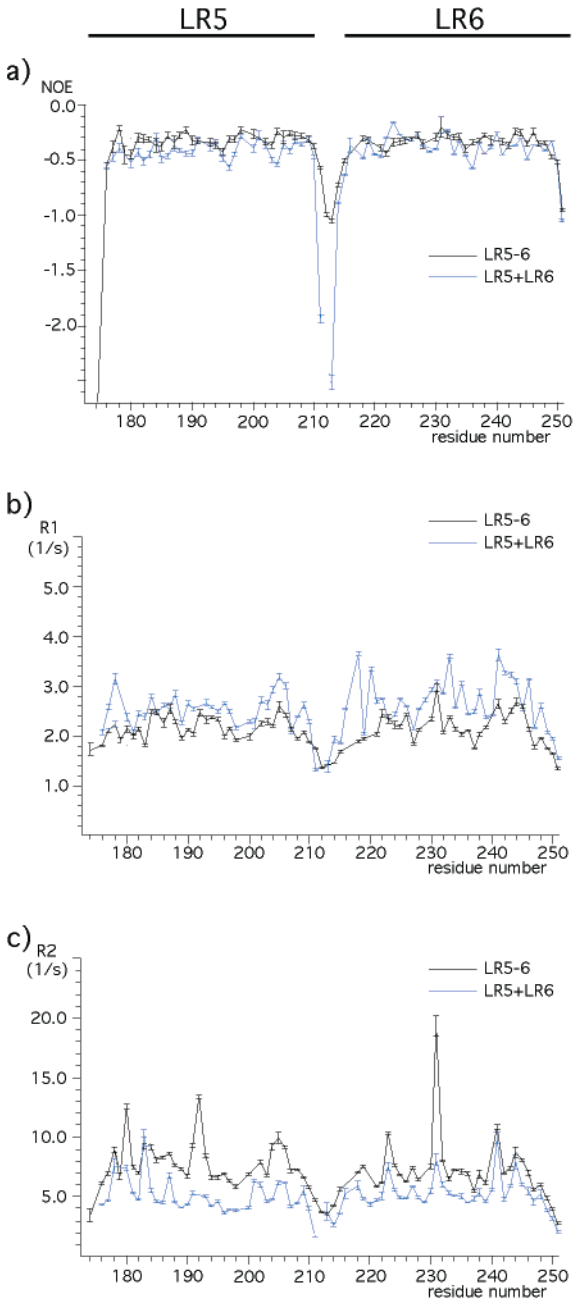

FIGURE 3: Comparison of the hNOE (a) and relaxation rates $R1$ (b) and $R2$ (c) for individual modules LR5 and LR6 with parameters for the LR5-6 pair. Rates are plotted as a function of residue number. Values for the individual modules LR5 and LR6 are illustrated in blue, and values for the LR5-6 module pair are indicated in black.

observed hNOE profile. The slower $R2$ relaxation rates for residues in the termini and the linker between repeats are also consistent with the large negative hNOEs and slow $R1$ relaxation rates.

To estimate the values of the order parameter for the linker residues, we used an approach previously employed by Campbell et al. (*32*, *34*). In Figure 4, the experimental T1 values are plotted against T2 relaxation times for the LR5-6 pair. Contour lines in the figure represent values of T1 and T2 calculated as a function of the Lipari-Szabo order parameter S^2 and overall correlation time τ_m using the simplest Lipari-Szabo model (*43*). It is clear from the plot that the residues in the linker (Ala211, Val212, Ala213,

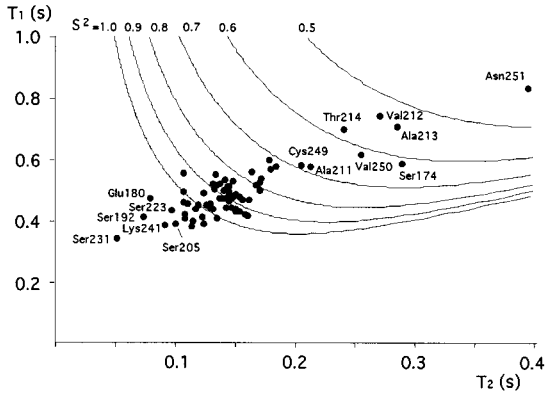

FIGURE 4: Distribution of $T1$ versus $T2$ relaxation times measured for the LR5-6 module pair. Errors for measured $T1$ values are 1.7 ± 0.8% (mean ± standard deviation), and errors for measured $T2$ values are 2.1 ± 1.0% (mean ± standard deviation). Contour lines in the figure represent values of $T1$ and $T2$ calculated as a function of the Lipari−Szabo order parameter S^2 and overall correlation time τ_m using the simplest Lipari−Szabo model (*43*). Labeled residues inside the $S^2 = 0.7$ boundary correspond to sites in the LR5-6 linker and in the N- and C-termini; labeled residues clearly outside the $S^2 = 1.0$ boundary, which also have elevated values of $J(0)$, are likely to be affected by slower (ms) time scale motions and are discussed in the text.

Thr214) and in both termini (Ser174, Val250, Asn251) have higher $T1$, $T2$ values than all other residues. The estimated order parameters for these residues are much lower than for the core residues, indicating a high degree of local flexibility.

Reduced Spectral Density Mapping Analysis. Because relative moments of inertia calculated from the X-ray structure of LR5 and from the minimized average structure of LR6 solved by NMR in solution are 1.0:0.82:0.60 and 1.0:0.79:0.54, respectively, anisotropic rotation of the individual modules is likely to take place. Therefore, we analyzed the relaxation data by spectral density mapping, which does not require any a priori assumptions about molecular geometry, type of rotational diffusion, or degree of internal motion. Reduced spectral density mapping is preferable to full spectral density mapping because experimental errors lead to artifacts in the calculated high-frequency components of the spectral density (*41*). Thus, in analysis using reduced spectral density mapping, the spectral density function at high frequencies, denoted $J_{avr}(w_H)$, is assumed to be flat.

Figure 5 compares the spectral density functions $J(0)$, $J(w_N)$, and $J_{avr}(w_H)$ calculated for each residue in LR5 and LR6 with those of the LR5-6 module pair. The average $J(0)$ is 1.1 ± 0.4 (ns/rad) for each individual module and is 1.8 ± 0.6 (ns/rad) for LR5-6. The overall correlation time, estimated from the expression $\tau_m = 5/2\langle J(0)\rangle$, is 2.75 ± 1.0 ns for LR5 and LR6 and is 4.50 ± 1.5 ns for each individual module in LR5-6. These estimated τ_m values are in good agreement with the correlation times of 2.8 ± 0.4 ns and 2.8 ± 0.6 ns (LR5 and LR6), and 4.6 ± 0.5 ns (LR5-6) calculated from $R2/R1$ ratios (1.9 ± 0.2, 1.9 ± 0.3 for LR5 and LR6, respectively, and 3.2 ± 0.4 for each module in LR5-6). Only residues that have hNOEs and $R2$ values within one standard deviation from the corresponding average values were included in calculations of $R2/R1$ ratios.

The observed τ_m for the LR5-6 pair is significantly lower than the correlation time predicted for this pair if the modules have a fixed relative orientation and tumble as a single structural unit (5.6 ns or greater depending on geometry).

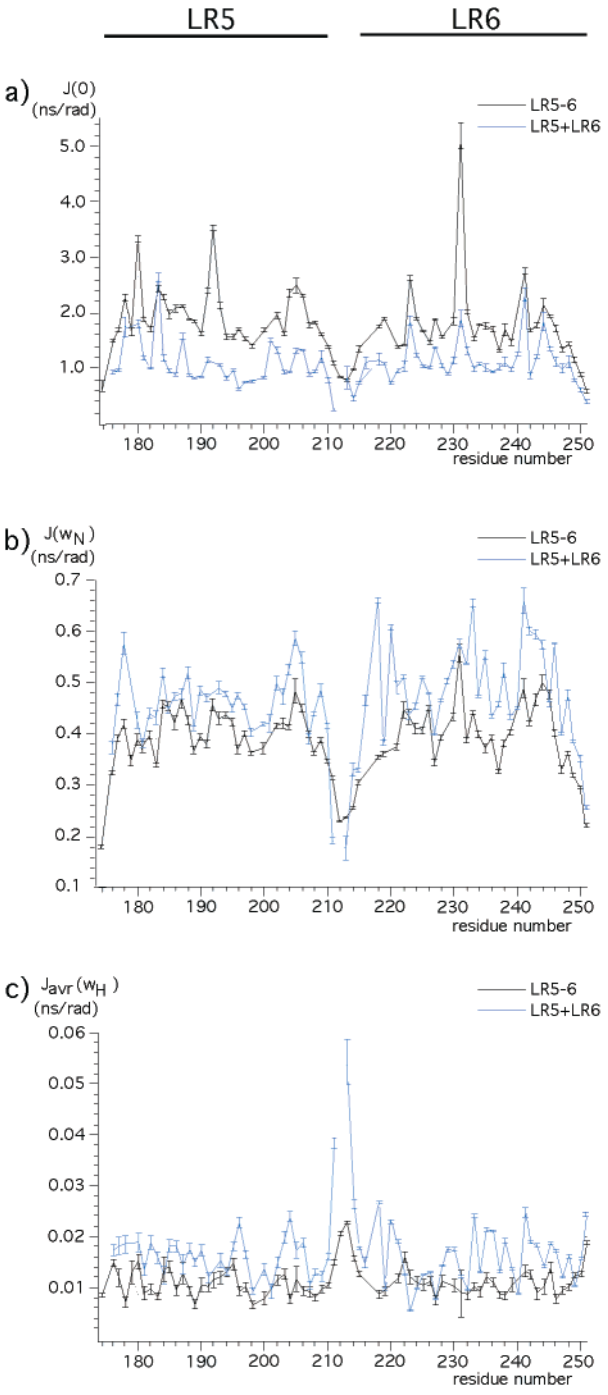

FIGURE 5: Reduced spectral density mapping of the individual modules LR5 and LR6 and of the LR5-6 module pair. The spectral density functions (a) $J(0)$, (b) $J(\omega_N)$, and (c) $J_{avr}(\omega_H)$ are plotted as a function of residue number. Values for the individual modules LR5 and LR6 are illustrated in blue, and values for the LR5-6 module pair are indicated in black.

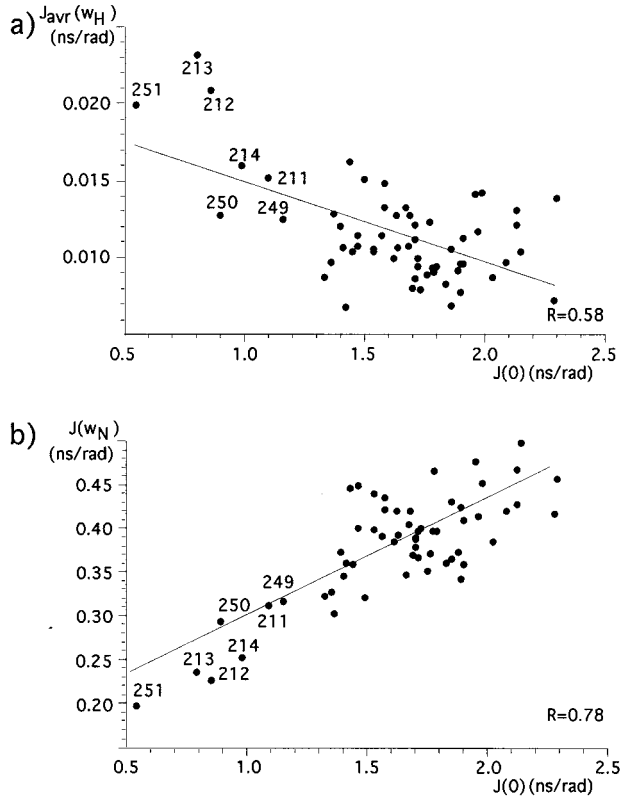

FIGURE 6: Correlation of the spectral density function $J(0)$ with (a) $J_{avr}(\omega_H)$ and (b) $J(\omega_N)$ for the LR5-6 module pair. The line shown is the best fit from least-squares regression analysis. The indicated residues, which have the lowest values of $J(0)$, all lie in the LR5-6 linker or at the C-terminal end of LR6.

Indeed, the overall correlation times of proteins with fixed interdomain orientations is usually much higher than the τ_m values of their individual domains, (e.g., refs *32* and *44*). An increase in the correlation time of the LR5-6 pair (as compared to each individual module) is likely a consequence of the spatial exclusion imposed by the presence of a second module attached to the first one by a short linker (*45*). Even for two modules connected by linkers of 25 and 50 residues undergoing uncorrelated motion, the value of τ_m increases when the individual modules are connected in the pair (*46*, *47*).

Residues at the N- and C-termini of the individual modules and the linker residues from 211 to 214 of LR5-6 have smaller than average values of $J(0)$, reflecting local flexibility (Figure 5, panel a). The decreased values of $J(0)$ for the linker are also consistent with the decreased $J(\omega_N)$ values and the elevated $J_{avr}(\omega_H)$ observed at these residues.

At a given residue, an increased contribution of high-frequency $J_{avr}(\omega_H)$ is characteristic of increased internal mobility. In the termini and linker, the decrease in $J(0)$ is accompanied by the expected increase in $J_{avr}(\omega_H)$ (Figure 6, panel a) and is well correlated with $J(\omega_N)$ (Figure 6, panel b). The overall shape of the spectral density function was further characterized using $J_{avr}(\omega_H)/J(0)$ ratios (*42*). For the core residues of LR5-6, $J_{avr}(\omega_H)$ contributes relatively little to the overall spectral density (0.6 ± 0.2%; average ratio ± SD). In contrast, the contribution of $J_{avr}(\omega_H)$ at the termini is much greater, with ratios ranging from 1.4 to 3.7%. The linker residues of LR5-6 also have increased $J_{avr}(\omega_H)/J(0)$ ratios with values of 1.4, 2.5, 2.9, and 1.6% for residues 211, 212, 213, and 214, respectively, reflecting an increased internal mobility of the linker.

Residues A178, E180, C183, E187, C201 of LR5, residues S223, S231, K241, S244 of LR6 and residues E180, C183, S192, S205, S223, S231, K241 of the LR5-6 pair have $J(0)$ values more than one standard deviation higher than the average (Figure 7). The elevated $J(0)$ values for these residues suggest the presence of conformational exchange.

FIGURE 7: Relaxation features of individual residues indicated on the primary sequence of LR5, LR5-6, and LR6. Open circles: residues with $(J(0)_i < \langle J(0)\rangle - 1.0*\mathrm{SD})$. Filled circles: residues with $J(0)$ values increased over average $(J(0)_i > \langle J(0)\rangle + 1.0*\mathrm{SD})$. Residues for which relaxation data could not be measured are indicated with backslashes that strike through the single letter amino acid code. The positions of calcium coordinating residues are indicated on the bottom row. Filled squares: coordination by side chain carboxylate group; open squares: coordination by backbone carbonyl group.

Sites in LR5 and LR6 that have increased $J(0)$ values correspond remarkably well with each other. For example, residues around the second and the fifth cysteine of each module (residues C183 and C201 of LR5; C222 and C240 of LR6) have an increased $J(0)$. The elevated values of $J(0)$ at or near these sites can be attributed to isomerization around the disulfide bond between the cysteines. There is no evidence of conformational exchange around the other two disulfide bonds. The increase in $R2$ observed for the backbone amides of S192 and S231, which occupy corresponding postions in modules 5 and 6, respectively, may result from ring flipping of adjacent histidine residues, which have their imidazole rings located within 5 Å of the affected amides in both modules. More generally, comparable positions of LR5 and LR6 have elevated $J(0)$ values. This finding indicates that similar residues have slow internal dynamics in LR5 and LR6. In the covalently bonded LR5-6 pair the residues with elevated $J(0)$ are essentially the same as in the individual modules (Figure 5, panel a), suggesting little change in the behavior of individual repeats when covalently connected.

DISCUSSION

The ligand-binding domain of the LDLR consists of seven contiguous LDL-A repeats, which are among the most common extracellular protein modules in the sequence database. Each of the seven adjacent LDL-A modules of the LDLR is connected to the next by a four-residue linker of variable primary sequence, except for modules four and five, which are connected by a 12-residue linker (*1*). Close homologues of the receptor, including the LRP, megalin, apoE-R2, and the VLDLR, also utilize similar arrangements of tandemly repeated LDL-A modules to bind ligands (*4*, *5*).

Although a wealth of structural information about individual LDL-A modules has accumulated, much less is known about whether the short linkers that connect adjacent modules impose any rotational constraints upon one module with respect to the next. We used NMR relaxation to analyze the overall and internal dynamics of the individual modules LR5 and LR6 and of the LR5-6 module pair to evaluate the amount of intermodular flexibility allowed by the four residue linker.

Several findings support the conclusion that the linker between LR5 and LR6 (i.e., residues 211−214) is highly flexible and that position of one module with respect to the other is not fixed. First, the experimentally measured hNOEs of the linker are decreased relative to the hNOEs of the core residues, as are the $R1$ and $R2$ relaxation rates. The estimated range of order parameters S^2 for the linker residues (Figure 4) are much lower than for the core residues. These estimated S^2 values are similar to order parameter values, extracted from a database of NMR-derived relaxation parameters, for flexible terminal residues of proteins (*48*).

Second, the linker residues also exhibit elevated values of $J_{avr}(w_H)$, which suggests increased high-frequency local motion. Furthermore, the spectral density function $J(0)$ decreases in the linker region of LR5-6, a finding that again is consistent with the presence of high-frequency internal motions in the linker. All of these properties change gradually from either end of the linker, reaching an extreme value at the two middle residues, which lie at positions 212 and 213 of the primary sequence.

Third, the pattern of internal dynamics in each module is very similar when the spectral density $J(0)$ values for residues from an isolated module are directly compared with $J(0)$ for the same residues in the module pair. When the value of $J(0)$ is increased in LR5 or LR6, it is also increased in the LR5-6 pair. Furthermore, the variation of $J(0)$ as a function of position in the amino acid sequence is similar in the individual modules and in the module pair, and the $J(0)$ profile of each individual module is essentially unchanged in the covalently connected LR5-6 pair, suggesting that one module exerts little influence on the internal dynamics of its neighbor in the LR5-6 pair.[2]

The four-residue linker, although short, is capable of separating the two modules by up to 15 Å when it is modeled in an extended conformation (Figure 8, panel a). Modeling calculations performed on a pair of fibronectin type III modules connected by a flexible poly(glycine) linker (*32*) reveal that linkers as short as two residues may permit unrestricted intermodular motions described by the "twist" angle (Figure 8, panel b), although the "tilt" of one module relative to the other can be affected even when a linker is 10 residues long (Figure 8, panel c). Restrictions resulting from direct spatial exclusion imposed by one module on its neighbor result in an observed small increase in the overall correlation time τ_m of the LR5-6 pair when compared with the τ_m values for the individual modules.

Other findings also support a model in which the LR5 and the LR6 modules act independently in the module pair. The Ca^{2+} affinity of LR5 is the same whether LR6 is covalently attached, and chemical shift perturbations occur primarily in the linker residues when LR5 and LR6 are covalently connected (*35*, *49*). Furthermore, no linker−

[2] The larger increase in $J(0)$ for S231 of the LR5-6 pair [as compared to the value of $J(0)$ for S231 in the single module] may result from minor differences in pH between the two NMR samples. Under the experimental conditions used (pH 5.6), even a change of only 0.1 pH unit could shift the populations of un-ionized and ionized histidine side chains, which have pK_a values near 6.0 when solvent-exposed, by about 6% in the vicinity of the affected serine. Given the known structures of the individual modules LR5 and LR6, it is highly unlikely that only the two serine residues at corresponding sites in modules five (S192) and six (S231) contact each other in the module pair and the relaxation properties of other residues do not change.

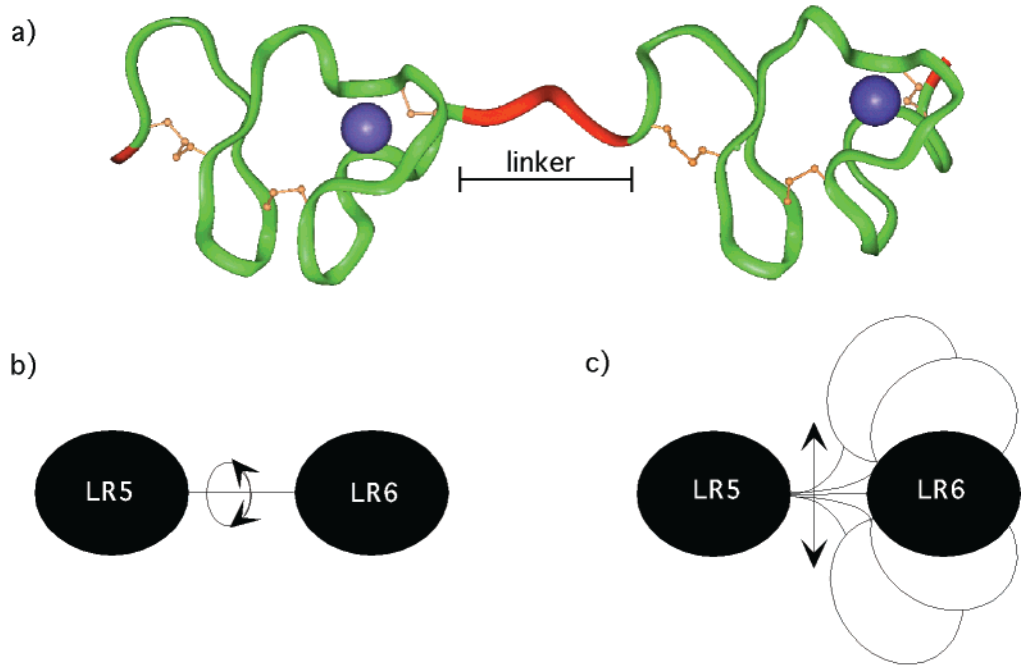

FIGURE 8: (a) Ribbon model of the LR5-6 pair showing the X-ray structure of LR5 (*22*) connected to the NMR structure of LR6 (*25*) by a flexible extended linker. Core residues of LR5 and LR6 are shown in green, flexible residues of the termini and linker are in red. Calcium ions are illustrated with violet spheres and disulfide bonds are shown in yellow. The flexibility of the linker allows essentially unrestricted rotation or "twist" (b). The bending or "tilt" (c) of one module with respect to the other is partially limited by spatial exclusion.

module or module−module NOE cross-peaks could be identified during the assignment procedure. The NMR relaxation data presented here, combined with these previous observations, strongly suggest that LR5 and LR6 do not adopt a fixed orientation with respect to each other in the LR5-6 pair.

Implications of Intermodule Flexibility for Receptor Function. The intermodule flexibility in the LR5-6 module pair (and in LR1-2) suggests that the structural relationship among individual LDL-A modules of the LDLR may resemble "beads-on-a-string." Such flexibility in the linker regions connecting individual modules will permit the ligand-binding repeats of the receptor to adjust their relative positions to bind a variety of heterogeneous apoE- and apoB-containing ligands of different particle shape, curvature, and diameter. The functional utility of maintaining flexibility in the linker connecting LDL-A modules contrasts sharply with the arrangement of EGF modules in fibrillin, where defined intermodule orientations establish elongated fibrills (*31*).

It is conceivable that the two-module system overlooks intermodule relationships that might exist in the context of the intact receptor (*50*−*52*). However, the short linkers connecting most LDL-A modules together in the LDLR makes it unlikely that distant modules can reach one another. Thus, we believe that the observed behavior of the LR5-6 module pair accurately reflects the inherent flexibility between these modules in the intact receptor.

ACKNOWLEDGMENT

We thank Dorothee Kern for helpful discussions, and we are indebted to Dr. Gerhard Wagner for use of NMR spectrometers at Harvard Medical School and the MIT/Harvard Center for Magnetic Resonance (supported by Grant RR00995 from the NIH) for use of NMR spectrometers housed at MIT.

REFERENCES

1. Yamamoto, T., Davis, C. G., Brown, M. S., Schneider, W. J., Casey, M. L., Goldstein, J. L., and Russell, D. W. (1984) *Cell 39*, 27−38.
2. Sudhof, T. C., Russell, D. W., Goldstein, J. L., and Brown, M. S. (1985) *Science 228*, 893−895.
3. Sudhof, T. C., Goldstein, J. L., Brown, M. S., and Russell, D. W. (1985) *Science 228*, 815−822.
4. Gliemann, J. (1998) *Biol. Chem. 379*, 951−964.
5. Willnow, T. E. (1999) *J. Mol. Med. 77*, 306−315.
6. Sakai, J., Hoshino, A., Takahashi, S., Miura, Y., Ishii, H., Suzuki, H., Kawarabayasi, Y., and Yamamoto, T. (1994) *J. Biol. Chem. 269*, 2173−2182.
7. Kim, D. H., Iijima, H., Goto, K., Sakai, J., Ishii, H., Kim, H. J., Suzuki, H., Kondo, H., Saeki, S., and Yamamoto, T. (1996) *J. Biol. Chem. 271*, 8373−8380.
8. Herz, J., Hamann, U., Rogne, S., Myklebost, O., Gausepohl, H., and Stanley, K. K. (1988) *EMBO J. 7*, 4119−4127.
9. Saito, A., Pietromonaco, S., Loo, A. K., and Farquhar, M. G. (1994) *Proc. Natl. Acad. Sci. U.S.A. 91*, 9725−9729.
10. Springer, T. A. (1998) *J. Mol. Biol. 283*, 837−862.
11. Brown, M. S., and Goldstein, J. L. (1986) *Science 232*, 34−47.
12. Goldstein, J. L., and Brown, M. S. (1974) *J. Biol. Chem. 249*, 5153−5162.
13. Herz, J., Clouthier, D. E., and Hammer, R. E. (1992) *Cell 71*, 411−421.
14. Hiesberger, T., Trommsdorff, M., Howell, B. W., Goffinet, A., Mumby, M. C., Cooper, J. A., and Herz, J. (1999) *Neuron 24*, 481−489.
15. Trommsdorff, M., Gotthardt, M., Hiesberger, T., Shelton, J., Stockinger, W., Nimpf, J., Hammer, R. E., Richardson, J. A., and Herz, J. (1999) *Cell 97*, 689−701.
16. Esser, V., Limbird, L. E., Brown, M. S., Goldstein, J. L., and Russell, D. W. (1988) *J. Biol. Chem. 263*, 13282−13290.
17. Russell, D. W., Brown, M. S., and Goldstein, J. L. (1989) *J. Biol. Chem. 264*, 21682−21688.
18. Beisegel, U., Schneider, W. J., Goldstein, J. L., Anderson, R. G. W., and Brown, M. S. (1981) *J. Biol. Chem. 256*, 11923−11931.

19. van Driel, I. R., Goldstein, J. L., Sudhof, T. C., and Brown, M. S. (1987) *J. Biol. Chem. 262*, 17443−17449.
20. Brown, M. S., and Goldstein, J. L. (1974) *Proc. Natl. Acad. Sci. U.S.A. 71*, 788−792.
21. Goldstein, J. L., Hobbs, H. H., and Brown, M. S. (1995) in *The Metabolic and Molecular Bases of Inherited Disease* (Scriver, C. S., Beaudet, A. L., Sly, W. S., and D., V., Eds.) pp 1981−2030, McGraw-Hill Inc., New York.
22. Fass, D., Blacklow, S., Kim, P. S., and Berger, J. M. (1997) *Nature 388*, 691−693.
23. Daly, N. L., Scanlon, M. J., Djordjevic, J. T., Kroon, P., and Smith, R. (1995) *Proc. Natl. Acad. Sci. U.S.A. 92*, 6334−6338.
24. Daly, N. L., Djordevic, J. T., Kroon, P. A., and Smith, R. (1995) *Biochemistry 34*, 14474−14481.
25. North, C. L., and Blacklow, S. C. (2000) *Biochemistry 39*, 2564−2571.
26. Huang, W., Dolmer, K., and Gettins, P. G. (1999) *J. Biol. Chem. 274*, 14130−14136.
27. Dolmer, K., Huang, W., and Gettins, P. G. (2000) *J. Biol. Chem. 275*, 3264−3269.
28. Blacklow, S. C., and Kim, P. S. (1996) *Nat. Struct. Biol. 3*, 758−762.
29. Atkins, A. R., Brereton, I. M., Kroon, P. A., Lee, H. T., and Smith, R. (1998) *Biochemistry 37*, 1662−1670.
30. Phan, I. Q. H., Boyd, J., and Campbell, I. D. (1996) *J. Biomolecular NMR 8*, 369−378.
31. Werner, J. M., Knott, V., Handford, P. A., Campbell, I. D., and Downing, A. K. (2000) *J. Mol. Biol. 296*, 1065−1078.
32. Spitzfaden, C., Grant, R. P., Mardon, H. J., and Campbell, I. D. (1997) *J. Mol. Biol. 265*, 565−579.
33. Bocquier, A. A., Potts, J. R., Pickford, A. R., and Campbell, I. D. (1999) *Struct. Fold Des. 7*, 1451−1460.
34. Smith, S. P., Hashimoto, Y., Pickford, A. R., Campbell, I. D., and Werner, J. M. (2000) *Biochemistry 39*, 8374−8381.
35. North, C. L., and Blacklow, S. C. (1999) *Biochemistry 38*, 3926−3935.
36. Bieri, S., Atkins, A. R., Lee, H. T., Winzor, D. J., Smith, R., and Kroon, P. A. (1998) *Biochemistry 37*, 10994−11002.
37. Kurniawan, N. D., Atkins, A. R., Bieri, S., Brown, C. J., Brereton, I. M., Kroon, P. A., and Smith, R. (2000) *Protein Sci. 9*, 1282−1293.
38. Pons, J.-L., Malliavin, T. E., and Delsuc, M. A. (1996) *J. Biomol. NMR 8*, 445−452.
39. Farrow, N. A., Muhandiram, R., Singer, A. U., Pascal, S. M., Kay, C. M., Gish, G., Shoelson, S. E., Pawson, T., Forman-Kay, J. D., and Kay, L. E. (1994) *Biochemistry 33*, 5984−6003.
40. Kay, L. E., Torchia, D. A., and Bax, A. (1989) *Biochemistry 28*, 8972−8979.
41. Dayie, K. T., Wagner, G., and Lefevre, J. F. (1996) *Annu. Rev. Phys. Chem. 47*, 243−282.
42. Peng, J. W., and Wagner, G. (1992) *Biochemistry 31*, 8571−8586.
43. Lipari, G., and Szabo, A. (1982) *J. Am. Chem. Soc. 104*, 4546−4559.
44. Bruschweiler, R., Liao, X., and Wright, P. E. (1995) *Science 268*, 886−889.
45. Nakaseko, Y., Neuhaus, D., Klug, A., and Rhodes, D. (1992) *J. Mol. Biol. 228*, 619−636.
46. Konrat, R., Krautler, B., Weiskirchen, R., and Bister, K. (1998) *J. Biol. Chem. 273*, 23233−23240.
47. Zhou, H., McEvoy, M. M., Lowry, D. F., Swanson, R. V., Simon, M. I., and Dahlquist, F. W. (1996) *Biochemistry 35*, 433−443.
48. Goodman, J. L., Pagel, M. D., and Stone, M. J. (2000) *J. Mol. Biol. 295*, 963−978.
49. North, C. L., and Blacklow, S. C. (2000) *Biochemistry 39*, 13127−13135.
50. Eck, M. J., Atwell, S. K., Shoelson, S. E., and Harrison, S. C. (1994) *Nature 368*, 764−769.
51. Xu, W., Harrison, S. C., and Eck, M. J. (1997) *Nature 385*, 595−602.
52. Sicheri, F., Moarefi, I., and Kuriyan, J. (1997) *Nature 385*, 602−609.

BI0027276